Focus Section: Volcano Monitoring in the Americas

Single-Station Multiparametric Seismic Monitoring of Copahue Volcano, Argentina–Chile (2018–2023)

José Augusto Casas[*1,2], Gabriela Alejandra Badi[2], Thomas Dylan Mikesell[3], Sebastian Esteban Garcia[4], and Deyan Draganov[5]

Abstract

Knowledge about the temporal evolution of a volcano is fundamental for an accurate understanding of the occurring physical dynamic processes and an appropriate assessment of the most probable near-future volcanic scenarios. Using seismic data recorded in the area of one of the most hazardous volcanoes along the Argentina–Chile, international border—Copahue volcano, we obtain information for an improved interpretation of the processes that occurred before, during, and after eruptive events. We use a single-station methodology to assess variations in the mechanical properties and internal structure of the Copahue volcano. Thus, we obtain information about structural alterations, friction and fractures, and variations in rigidity in the volcanic system. Our results show that the time variations of the evaluated seismic parameters correlate to the volcanic phenomena observed on the surface, that is, incandescence and ash emissions. Accounting for the physical processes, to which the analyzed seismic parameters are sensitive, and previous models developed for the area, we propose a physical model explaining the eruptive events that occurred at Copahue in the period 2018–2023. This model can potentially be used for the assessment of future scenarios, which is of fundamental importance for the institutions in charge of the real-time monitoring of Copahue volcano to improve the quality of their evidence-based decisions.

Cite this article as Casas, J. A., G. A. Badi, T. D. Mikesell, S. E. Garcia, and D. Draganov (2024). Single-Station Multiparametric Seismic Monitoring of Copahue Volcano, Argentina–Chile (2018–2023), *Seismol. Res. Lett.* **XX**, 1–14, doi: 10.1785/0220240074.

Supplemental Material

Introduction

Early warnings are a key element in reducing volcanic risk. Volcano observatories implement methodologies to effectively describe the current state of volcanic systems and anticipate hazardous volcanic phenomena (Ewert and Swanson, 1992; Aspinall and Blong, 2015). Although the major geological processes that lead to the formation of volcanoes are well understood, the volcanic systems exhibit unique dynamics caused by the complex relationship between their constituent materials and the structural setting shaped by their geological history. This complex dynamics leads to high uncertainty in classifying the volcanoes as likely or not to erupt within a short time (Papale, 2020).

Seismic signals are the main source of information for evaluating volcano dynamics. Because fluids (magma, gases, and meteoric water) move in the system, fractures are created or reactivated, pressure and temperature change, and the composition of some fluids varies. Each of these changes produces seismic signals (McNutt, 2005). Traditionally, monitoring a magmatic system has been carried out through the identification and localization of seismic sources, signals for which are recorded by instruments deployed in the local area of influence (Battaglia *et al.*, 2005; Thompson *et al.*, 2015; Bueno *et al.*, 2019). Through this approach, the evolution of a system can be interpreted based on the quantity, magnitude, spatio-temporal distribution, and physical mechanisms associated with the diverse types of seismic events occurring in volcanic areas. In such a way, volcano tectonic (VT), long-period (LP), and tremor events (among the most often identified types of volcanic events) can provide information relevant to rock fracture, fluid movement, and resonance phenomena in cracks (McNutt, 2005). However, because not all subsurface processes

1. Servicio Geologico y Minero Argentino (SEGEMAR), CONICET, Buenos Aires, Argentina, https://orcid.org/0000-0002-6190-157X (JAC); 2. Facultad de Ciencias Astronomicas y Geofisicas, Universidad Nacional de La Plata, La Plata, Argentina, https://orcid.org/0000-0003-0512-1015 (GAB); 3. Norwegian Geotechnical Institute, Oslo, Norway, https://orcid.org/0000-0001-9900-9846 (TDM); 4. Observatorio Argentino de Vigilancia Volcanica (OAVV), Servicio Geologico y Minero Argentino (SEGEMAR), Buenos Aires, Argentina, https://orcid.org/0000-0002-9528-3634 (SEG); 5. Department of Geoscience and Engineering, Delft University of Technology, Delft, The Netherlands, https://orcid.org/0000-0001-8606-1178 (DD)

*Corresponding author: augusto.casas@segemar.gov.ar

are associated with distinguishable seismic events, using just a limited part of a seismogram leads to an incomplete understanding of the dynamic processes occurring in the subsurface.

As a response to this challenge, the complete seismic records have been extensively used to describe the temporal evolution of a magmatic system (Endo and Murray, 1991; Kumagai *et al.*, 2010; Bueno *et al.*, 2021; Rey-Devesa *et al.*, 2023). These methods and techniques have markedly increased the amount of information obtained about the structures and processes occurring in the subsurface (Rey-Devesa *et al.*, 2023). The complete seismic data recorded by stations (or a station) located in an area of interest can be used to monitor changes occurring in the subsurface (Lesage, 2022). To accomplish this goal in a volcanic environment with limited station coverage, we evaluate selected physical parameters sensitive to structural alterations, friction and fractures, and subsurface rigidity (namely, the horizontal-to-vertical spectral ratio [HVSR], real-time seismic amplitude measurements [RSAM] and frequency index, and relative seismic velocity variations, respectively). Based on a single-station approach, according to which the recordings of a three-component station are used, we characterize the variations in the subsurface in the vicinity of the station.

The target volcanic system is classified as one with the highest risk in Argentina and Chile—Copahue volcano (Elissondo and Farıas, 2024; SERNAGEOMIN, 2024). We propose a methodology for monitoring Copahue representing the joint interpretation of the results from four methods. Based on single-station three-component records, we demonstrate that this methodology provides valuable information to describe the temporal evolution of the Copahue volcano. This information is of relevance for understanding the workings of the analyzed dynamic magmatic system.

Case Study: Copahue Volcano

Copahue volcano (see location in Fig. 1) is the current eruptive structure of the Caviahue–Copahue volcanic complex. This volcanic complex is characterized by a significant interaction between tectonics, volcanic activity, and the local geothermal field (Folguera *et al.*, 2016; Barcelona *et al.*, 2019; Tardani *et al.*, 2021). This is evidenced by the volcanic manifestations not only within the active crater and the volcano edifice but also throughout its associated geothermal field (Agusto *et al.*, 2018). In this area, the main cause of eruptions is not the differentiation of long-lived magma volumes (as in many volcanic systems along the Andes) but the mixing of new and emplaced magmas (Stern, 2002).

Copahue is the highest-risk volcano in Argentina (Elissondo and Farıas, 2016) and the eighteenth-riskiest in Chile (SERNAGEOMIN, 2024). This volcanic system has produced around 15 small eruptions (VEI 1 to 2) in the last 250 yr (Caselli, Liccioli, and Tassi, 2016; Caselli, *et al.*, 2016). The towns affected most by this activity are Copahue and Caviahue, which are 5 and 9 km from the volcano, respectively (Caselli, Liccioli, and Tassi, 2016; Caselli, *et al.*, 2016). The Copahue volcano is monitored by the Observatorio Volcanológico de los Andes del Sur (OVDAS) and the Observatorio Argentino de Vigilancia Volcánica (OAVV). OVDAS and OAVV perform seismic, geochemical, geodetic, and remote-sensing monitoring, as well as real-time visual inspection. The information collected by these institutions is then interpreted and published in Volcanic Activity Reports, the periodicity for which is related to the level of activity of the volcanoes (SEGEMAR, 2024; SERNAGEOMIN, 2024).

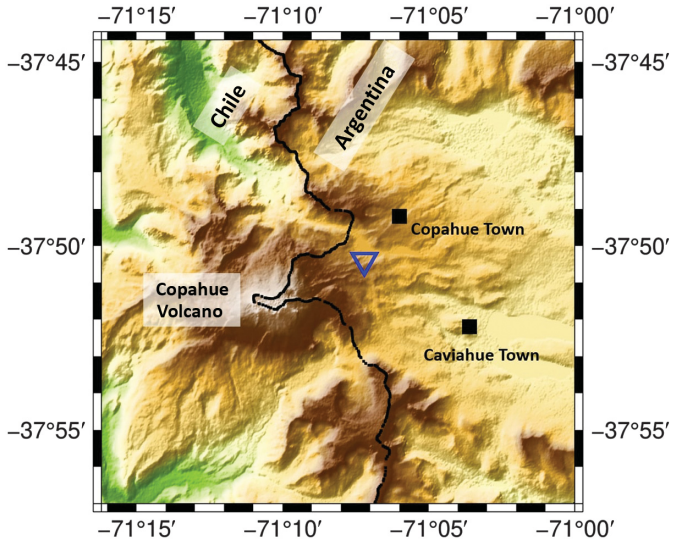

Figure 1. Location of Copahue volcano, the closest towns, and the seismic station MLZ (upside-down triangle) used for processing.

The latest eruptive cycle of the Copahue volcano started in 2012 (Agusto *et al.*, 2017). This period displayed phreatic and phreatomagmatic activity with maximum gas and ash columns of 1.9 and 2.5 km, respectively, and a broad range of seismic activity (SEGEMAR, 2024; SERNAGEOMIN, 2024). Examples of the most recent less-energetic eruptive phases during this period are the phreatic eruptions that started in July 2018, September 2019, June 2020, July 2021, and November 2022, which were characterized by maximum ash columns between 1.2 and 1.74 km above the crater together with the intervals of incandescence (that is, luminosity originated by high-temperature releasing gases).

Based on seismic, geochemical, deformation, and meteorological data, the complementary subsurface models for the Copahue volcano were developed (Ibáñez *et al.*, 2008; Lundgren *et al.*, 2017; Carbajal *et al.*, 2022; Farias *et al.*, 2023; Astort *et al.*, 2024). Lundgren *et al.* (2017) suggested the system to be composed of a deep reservoir located below the CCVC caldera (around 10 km depth) supplying magma to a shallow reservoir below the crater at Copahue (at 2.5 km depth). Farias *et al.* (2023) used seismic data recorded around the Copahue volcano to estimate the *b*-value of the

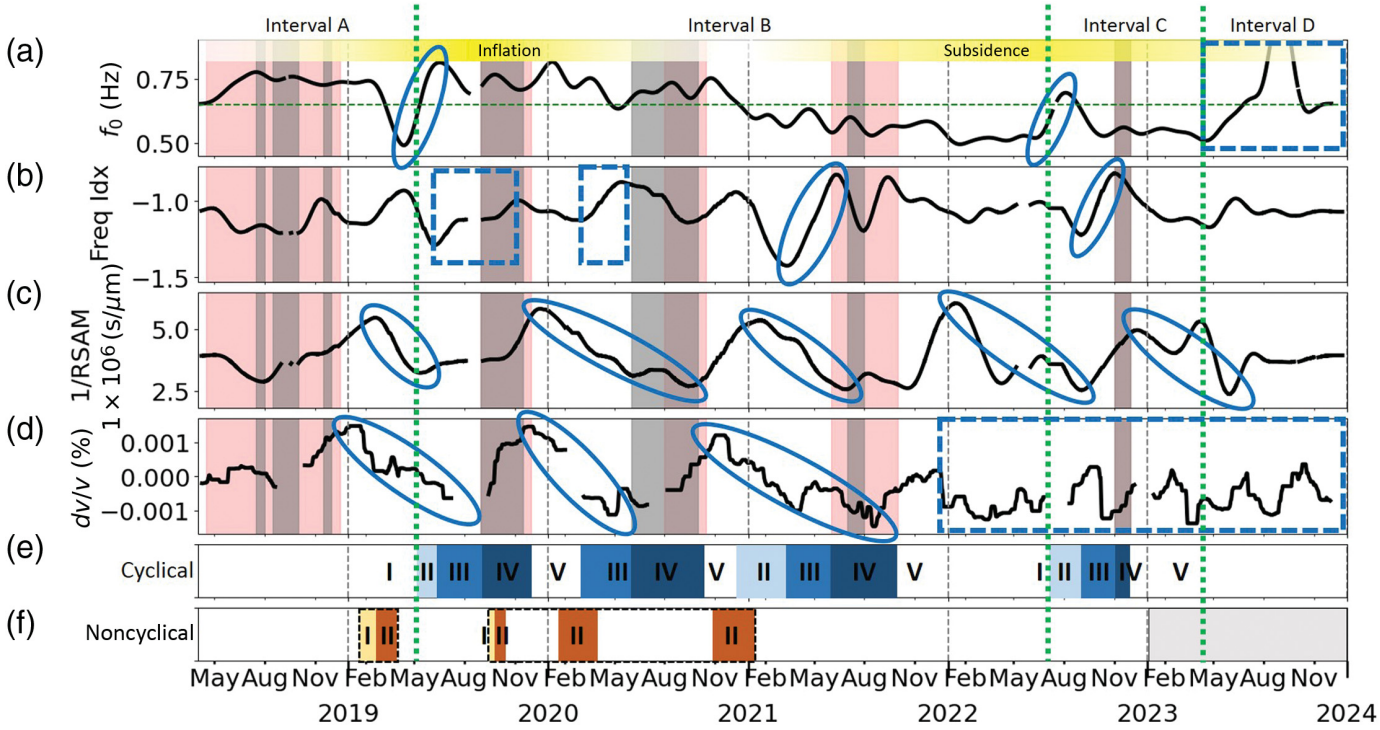

Figure 2. Evolution of the evaluated seismic parameters in the analyzed period: (a) fundamental frequency (f_0); (b) frequency index (Freq Idx); (c) reciprocal of the real-time seismic amplitude measurement (1/RSAM); (d) relative seismic velocity variations (*dv/v*); (e) stages of the cyclical processes as in the proposed physical model; and (f) stages of the noncyclical processes as in the proposed physical model. For f_0, frequency index and 1/RSAM, low-pass filtered (for periods larger than 2 months) curves are shown. The green dashed vertical lines indicate the boundaries between the interpreted intervals based on the evolution of f_0. In panel (a) a horizontal dashed line indicates the median f_0 value. At the top of panel (a), the intervals characterized by inflation and subsidence are indicated (Astort *et al.*, 2024). Relevant features along the curves are indicated with ellipses and squares; for a given seismic parameter, ellipses indicate a repeated pattern, and dashed rectangles indicate inconclusive (see Freq Idx) and non-repeated (see f_0 and *dv/v*) anomalous features. As a reference, gray shaded areas indicate the intervals in which ash columns and incandescence were reported by the local governmental institutions, and red shaded areas indicate intervals with only incandescence. For the cyclical processes in panel (e), the green vertical dashed line indicates stage I, and stages II–IV are indicated with blue scale, and stage V is indicated in white between stage IV and stage I; for the noncyclical processes in panel (f), stages I and II are indicated with orange scale and the interval with no results is in gray (Farias *et al.*, 2023).

Gutenberg–Richter law over time (Gutenberg and Richter, 1944), providing a measure of variations in the state of stress in the volcanic system (Scholz, 2015). Based on an interpretation of the results of the *b*-value and the nature and depth of the seismicity in the area, they infer several instances of rock fracturing and/or opening of cracks as well as instances of fluid flow in the hydrothermal system (indicated with light and dark orange in Fig. 2f, respectively, for the interval 2019–2023). Based on the ground deformation time series, Astort *et al.* (2024) indicated that inflation occurred in the system during the period 2018–2020, which was followed by subsidence in 2021–2023 (see Fig. 2a). Carbajal *et al.* (2022) proposed that the volcanic phenomena occurring in 2019–2023 at Copahue is regulated by seasonal variations. Weather conditions and surface processes (e.g., snow melting) influence the dimensions of the crater lake, leading to processes of chemical precipitation (Carbajal *et al.*, 2022). This process affects the fluid pressure in the hydrothermal system, developing periodic phreatic eruptions.

Copahue volcano has been cooperatively seismically monitored from both Argentina and Chile after governmental institutions agreed on the deployment of a binational seismic network. Currently, the OAVV and OVDAS maintain eleven seismic stations deployed in the area of Copahue. In this study, from the stations located in Argentina, we use the one closest to the crater and with a sufficiently long recording time to analyze the volcanic phenomena that occurred between 2018 and 2023, that is, MLZ station (see location in Fig. 1). We use seismic data recorded by MLZ to characterize the subsurface processes that occurred before, during, and after the eruptive episodes observed in the period 2018–2023.

Multiparametric Approach

Volcano observatories seek the most effective tools for the detection of anomalous volcanic phenomena (Ewert and Swanson, 1992). Changes observed in selected seismic parameters might indicate a variation in the physical state of the volcanic system (Sparks *et al.*, 2012). The observed changes are related to the physical processes to which the corresponding seismic

parameters are sensitive, contributing to understanding the current volcano dynamics (Scarpa *et al.*, 1996; Machacca *et al.*, 2023). The number and type of physical parameters used for monitoring affect the quality of the extracted information as well as the timing in which the interpretations can be performed. Although there are many seismic parameters, using a limited quantity of effective nonredundant parameters is fundamental for an appropriate examination of the seismic records (Cortés *et al.*, 2015). Thus, volcano observatories explore the parameters most sensitive to the changes that occur in each specific monitored volcanic system (Pallister and McNutt, 2015).

A comprehensive monitoring describes the evolution of the internal structure and mechanical properties of a complex volcano system. Effective monitoring can be achieved through the analysis of the variations in time of the three fundamental physical parameters: structural alterations, friction and fractures, and rigidity (Le Breton *et al.*, 2021). In this work, we explore these three physical parameters using the full seismic data recorded near Copahue volcano during the interval 15 April 2018–15 December 2023. Of the seismic methods that are sensitive to these three physical parameters, we select four methods widely used by the scientific community for monitoring purposes, namely, HVSR, RSAM, frequency index, and relative seismic velocity variations. We combine them into a proposed methodology to describe the evolution of Copahue during the analyzed time interval.

In the following subsections, we introduce the applied methods and relate their results to the observed volcanic phenomena. In the last subsection, we collate and compare the results obtained for each technique. Figure 2 shows the evolution of the evaluated seismic parameters. For each of the seismic parameters, a systematic occurrence of a specific anomalous feature (i.e., a pattern) is indicated by ellipses. Furthermore, the dashed rectangles indicate the intervals characterized by anomalous but nonrepeated (see Fig. 2a,d) or ambiguous (see Fig. 2b) features in the analyzed period.

HVSR

Several seismic methods are extensively applied for the exploration of subsurface structures. One of them is the HVSR method, first proposed for site-effect exploration (Nakamura, 1989). According to this method, the ratio between the horizontal and vertical spectral amplitudes of the motion recorded by a seismometer at the surface can be used to estimate the fundamental frequency (f_0) of a volume around the station (roughly, within a radius of one wavelength for a related frequency) (Okamoto and Tsuno, 2018).

Spatial variations of HVSR have been reported as caused by anomalous structures (Satoh *et al.*, 2001; Khalili and Mirzakurdeh, 2019). Spatially, the dense observations of HVSR can reveal local variations in subsurface structures (Nishitsuji *et al.*, 2014; Gosar, 2017). However, temporal variations of HVSR are scarcely reported (Okamoto *et al.*, 2021).

The HVSR method can be applied using ambient seismic noise. Because of the randomness of the noise wavefield, the position and attributes of the noise sources might change in space and time, thus affecting the estimation of HVSR. In these unfavorable situations, the results from HVSR could be unstable: the HVSR curves obtained for different times of the day might significantly differ in amplitude and shape; the estimated fundamental frequency could also deviate (Cipta *et al.*, 2018). Moreover, environmental noise sources like wind and rain could introduce nonnegligible errors to the calculations. Because of all these factors affecting the stability of the calculations, a robust statistical method should be used for HVSR calculations (Xu and Wang, 2021).

To address these issues, we perform HVSR calculations using *hvsrpy*—an open-source Python package for HVSR processing based on a statistically robust approach (Cox *et al.*, 2020). *hvsrpy* uses a lognormal distribution to describe the resulting resonant frequency values; the algorithm can reject deficient windows to effectively decrease the variance of the results and improve the quality of the data (Acerra *et al.*, 2004) (an example of the results obtained for arbitrarily chosen days can be found in Fig. S1, available in the supplemental material to this article).

We use *hvsrpy* to analyze the evolution of the statistically obtained fundamental frequency (from here on, named as f_0) between April 2018 and December 2023. The curve in Figure 2a shows f_0 in the analyzed period. To remove the high-frequency small-amplitude variations, Figure 2a shows a low-pass filtered (for periods larger than 2 months) curve (see the nonfiltered results in Fig. S2a). The results evidence a median f_0 of 0.64 Hz and a median standard deviation of 0.10 Hz; then, variations of f_0 higher than the obtained deviation are statistically significant, which we interpret as caused by changes in the volcanic system.

In general terms, between April 2018 and December 2023, f_0 shows a slow decrease in its values. Based on the rate of the decreasing trend, the f_0 curve suggests two contiguous intervals, that is, 2018–2020 with a median f_0 of 0.72 Hz and 2021–2023 with a median of 0.56 Hz. Furthermore, along the f_0 curve, four intervals can be distinguished (see the vertical dashed lines in Fig. 2 and also in Fig. S2): interval A, April 2018–May 2019; interval B, May 2019–July 2022; interval C, July 2022–April 2023; and interval D, April 2023–December 2023.

The intervals A–C are characterized by a monotonous decrease of f_0; these are separated by a rapid increase in the values of f_0. The last interval (D) is defined by transient anomalously high-f_0 values (in an average, 0.74 Hz), which disappear by December 2023.

Only intervals B and C, out of all the distinguished intervals, are fully contained within the recording period. These two intervals show a pattern characterized by a rapid increase in the values of f_0 that breaks the monotonously decreasing trend of the curve, which is followed by ash emissions a few months later: for interval B, ash emissions were recorded ~4 months

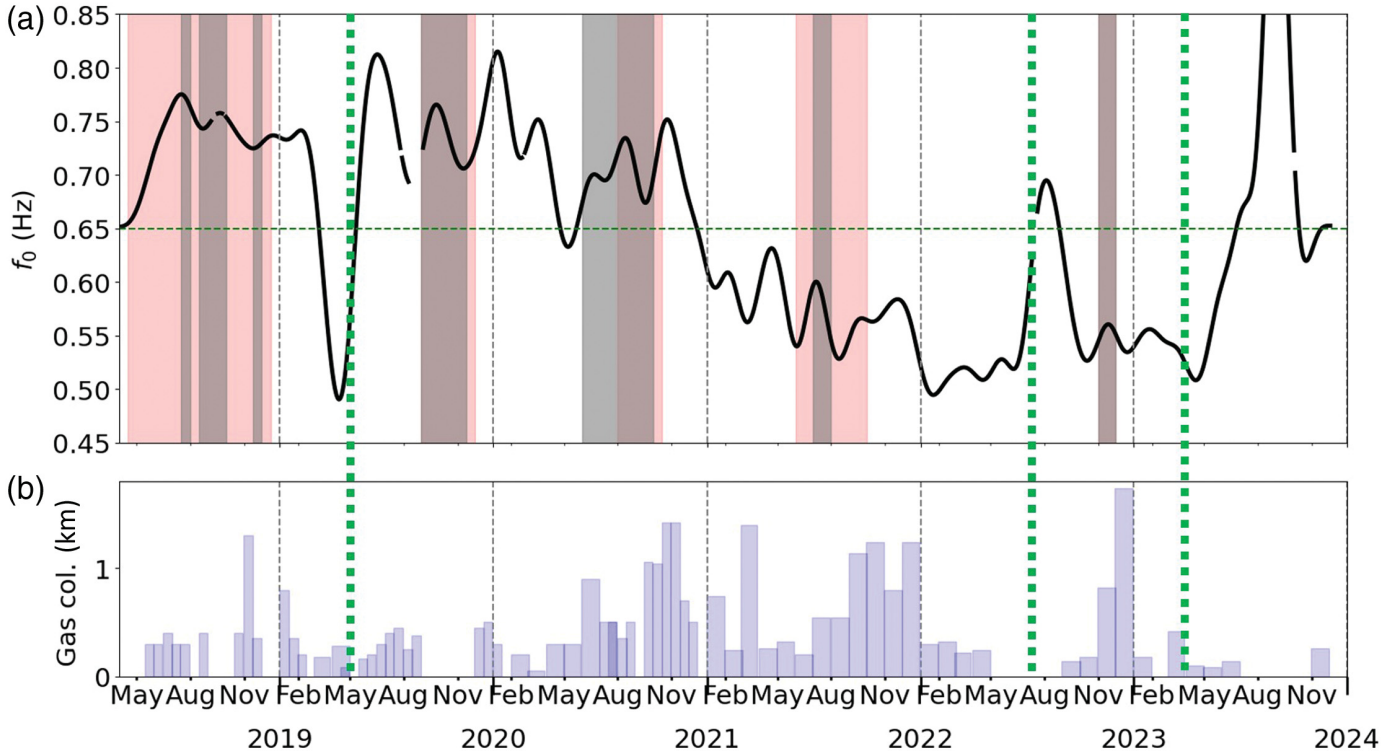

Figure 3. (a) Evolution of the statistical fundamental frequency (f_0) obtained for MLZ station during April 2018–December 2023. The curve shows a low-pass filtered (periods larger than 2 months) curve of the f_0 values obtained for each day. As a reference, gray shaded areas indicate the intervals in which ash columns and incandescence were reported by the local governmental institutions, and red shaded areas indicate intervals with only incandescence. (b) Height of gas columns reported by OVDAS and OAVV (SEGEMAR, 2024; SERNAGEOMIN, 2024). The green dashed vertical lines indicate the boundaries between the intervals with decreasing f_0 values followed by a rapid increase in f_0 during the analyzed period.

later, and for interval C, ~5 months later. Although new ash columns were reported in June 2020 and July 2021 (that is, during interval B), no previous significant variations were detected along the f_0 curve. We infer that such precursory signals are missing or below the threshold of detection.

Conceptually speaking, an increase (decrease) of f_0 in a system is caused by an increase (decrease) of its volumetric mass or its density or by a decrease (increase) of its damping (Moore *et al.*, 2018). At the seismological scale, higher (lower)-f_0 values are usually interpreted as originating by stiffening (softening) of the subsurface below a station, caused by multiple reasons such as an increase (decrease) of the pressure field in the system or variations in the composition of subsurface elements (Bour *et al.*, 1998; Mundepi *et al.*, 2009; Torrese *et al.*, 2020). Analyses of the deformation processes that occurred around Copahue indicate an inflation during the interval 2018–2020 and a subsidence during 2021–2023 (Astort *et al.*, 2024). We interpret the higher f_0 median in the interval 2018–2020 as caused by a transient higher pressure in the volcanic system originating the inflation; similarly, we interpret the lower f_0 median observed in the interval 2021–2023 as caused by a decrease of the pressure in the subsurface due to subsidence.

The distribution of gas columns along the analyzed period indicates that the boundaries between the interpreted intervals occur during periods characterized by low gas emissions (see Fig. 3). Carbajal *et al.* (2022) proposed that the sequence of water deficiency and oversupply in the hydrothermal system caused by seasonal weather variations (i.e., snow on the surface in winter and melted water percolating into the system during warmer seasons) results in episodes of chemical precipitation that obstruct near-surface conduits. These episodes of obstruction would increase the local pressure, resulting in higher f_0 values. Based on an analysis of the obtained f_0 values, the heights of the gas columns for the same period (SEGEMAR, 2024; SERNAGEOMIN, 2024), and considering the chemical precipitation processes occurring in the area, we interpret the rapid increase in f_0 obtained in our results as indicative of episodes of subsurface conduit obstruction.

Frequency index

Frequency index is a relevant seismic parameter for describing active volcanic systems (Buurman *et al.*, 2006). The frequency index is computed as $\mathrm{FI} = \log_{10}\left(\frac{A_{\mathrm{high}}}{A_{\mathrm{low}}}\right)$. This parameter describes the relation between the spectral content of a given signal at high and low frequencies. Through a selection of the range of frequencies composing the high- and low-frequency bands, A_{high} and A_{low} are computed as the average spectral amplitude for the higher and lower frequencies, respectively.

Even though the frequency index has been mainly employed to efficiently classify the seismic events by means of their spectral attributes, the frequency index can be used to analyze any recorded time window offering a tool for monitoring spectral variations along the records (Ketner and Power, 2013).

We use the vertical-component records of MLZ station, for which instrument-response correction, demeaning, and detrending are applied. Provided the typical range of frequencies of the processes relevant to fluid flows and rock fractures (McNutt, 2005; Wassermann, 2012) for the computation of the frequency index values, we select a low-frequency band of 0.8–2 Hz and a high-frequency band of 4–10 Hz. Using 10 min nonoverlapping windows, we compute the frequency index values taking the median of the spectral amplitudes for the selected high- and low-frequency bands.

Figure 2b shows the low-pass filtered (for periods larger than 2 months) frequency index values obtained for the analyzed time period (see the nonfiltered results in Fig. S2b). The frequency index curve shows significant variations for the time of the eruptive events that occurred during the analyzed period, characterized by a local minimum followed by a local maximum (note that only the increasing part of this feature is indicated in Fig. 2b). This feature is evident for the time before the volcanic events observed in 2021 and 2022 (see blue ellipses in Fig. 2b); however, it is harder to distinguish in 2019 and 2020 (see blue dashed rectangles in Fig. 2b).

A gap of data (occurred during the last 3 weeks of August 2019) was present a week before the ash emissions in September 2019. During the period prior to this volcanic event, the curve shows a local minimum when a local maximum is not observed. Even though this gap of data does not affect the long-term trend of the curve, it increases the uncertainty on the interpretation. Observing the tendency of the curve during such an interval, we speculate that, were the data complete, the frequency index curve would have kept increasing to develop the missing maximum. In addition, during the time before the ash column started in June 2020, the gentle local minimum and maximum values are observed.

An increase (a decrease) along the frequency index curve is caused by a transient higher energy at higher (lower) frequencies compared to the lower (higher) frequencies. Because the observed pattern occurs after the features observed along f_0 and before ash columns and incandescence (see Fig. 2), we interpret the drops along the frequency index curve as relevant to more energetic low-frequency events, likely caused by an increase of the flow of fluids in the hydrothermal system. The increased flow of fluids would cause an increase in the local pressure, which reduces the effective pressure in the system and, consequently, leads to a process of local opening of cracks; we interpret the increasing frequency index values as caused by the progressive increase in the high-frequency energy associated with this process (Bolton *et al.*, 2022).

RSAM

The energy recorded by seismic instruments deployed around an active volcano is indicative of the level of activity of the volcanic system. RSAM (Endo and Murray, 1991) is a method widely used among worldwide volcano observatories to estimate the energy released by an active system. RSAM applied to the sequential time windows provides estimates of the variations of the seismic energy released by an active volcanic system (Qamar *et al.*, 2008). The acceleration of RSAM with time has been shown to be a valuable indicator of an imminent eruption (Cornelius and Voight, 1994, 1996; Chardot *et al.*, 2015). Then, to efficiently identify the major variations, its reciprocal (i.e., 1/RSAM) is commonly used (Cornelius and Voight, 1996; Sparks, 2003).

We use the vertical-component records of MLZ station to compute RSAM. Daily seismic data are corrected for instrument response, detrended, and demeaned. Data are also band-pass filtered between 0.2 and 10 Hz—a frequency range above the microseism energy and below the most energetic weather influences. Then, we compute RSAM for 10 min nonoverlapping windows by taking the mean of its envelope. Finally, we use 1/RSAM to analyze the evolution of Copahue volcano in the period April 2018–December 2023.

Figure 2c shows the low-pass filtered (for periods larger than 2 months) 1/RSAM curve obtained for the analyzed period (see the nonfiltered curve in Fig. S2c). These results show local minima occurring in an interval (in average, 2 months) previous to ash emissions.

The 1/RSAM results appear to show an annual pattern. To test that, we compare these results with weather parameters for the period analyzed (that is, precipitations and temperatures) (Funk *et al.*, 2015; Rivera *et al.*, 2018; Climate-Hazards-Center, 2020; Verdin *et al.*, 2020). This seismic parameter presents the local minimum values during the maximum precipitations and minimum temperatures along each year (see Fig. 4).

Some physical models describe the seismic signals originated by the subsurface fluid dynamics (Girona *et al.*, 2019); fluid flows and accumulation of fluids cause pressure oscillations in the volcanic system, which are recorded by the nearby seismic instruments as changes in amplitudes along the time and frequency. We interpret the significant correlation of 1/RSAM and the weather parameters at Copahue (see correlation values in Table 1) as indicating that 1/RSAM values describe the general condition of the hydrothermal system.

1/RSAM presents an above-average correlation to precipitations. Higher precipitation increases the amount of fluids contained in the hydrothermal system. Depending on the subsurface structures, the already present fluids, and the pressure in the system, the penetrating fluids create new accumulation zones and fluid flows. The percolating water flows in the hydrothermal system filling the pore space in a process controlled by the properties of the subsurface materials. The new subsurface conditions alter the stress state in the system

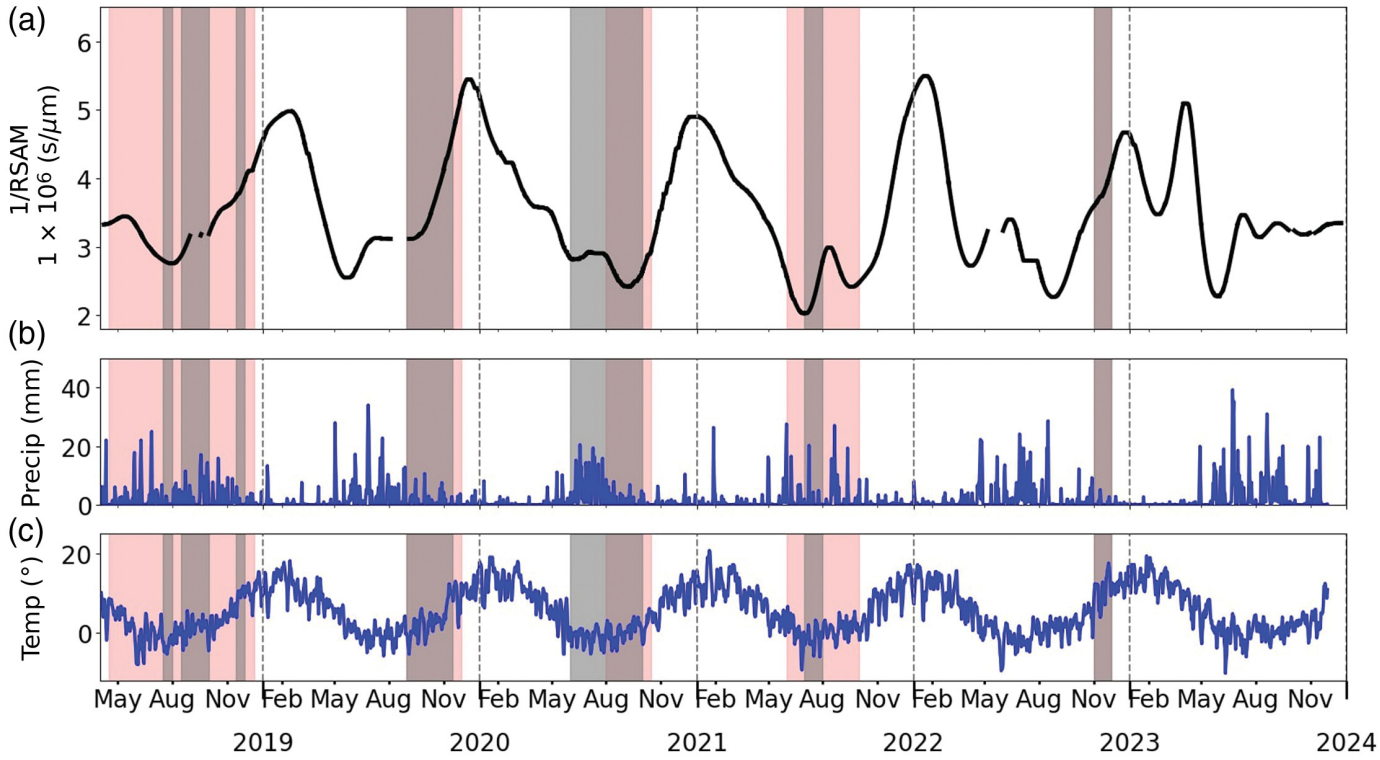

Figure 4. (a) Evolution of 1/RSAM obtained for MLZ station during April 2018 to December 2023. The curve has been low-pass filtered for periods larger than 2 months. As a reference, grey shaded areas indicate intervals in which ash columns were reported by OVDAS and OAVV, and red-shaded areas indicate intervals with incandescence. (b,c) Evolution of two weather parameters such as precipitations and temperature (Funk *et al.*, 2015; Rivera *et al.*, 2018; Climate-Hazards-Center, 2020; Verdin *et al.*, 2020).

causing variations in the recorded seismic field. Note that, depending on the released seismic energy during this process, the variations might not be recorded as isolated detectable seismic events. We interpret that the processes caused by the increased amount of fluids in the hydrothermal system are manifested in the 1/RSAM.

Relative seismic velocity variations

The ambient seismic field has been extensively used in recent decades to measure seismic velocity variations, particularly in volcanic environments (Obermann *et al.*, 2013; Sens-Schonfelder and Brenguier, 2019; Cabrera-Pérez *et al.*, 2023). Green's functions can be estimated using different time windows at the same location. Then, phase shifts in the retrieved coda waves are exploited to estimate changes in the propagation velocity in the medium (Snieder *et al.*, 2002; Snieder, 2006).

Provided the efficiency of multiple scattered waves to sample the medium of interest, coda waves have high sensitivity to small changes in the medium so that even weak velocity changes (even less than 10^{-3}%) are detectable (Weaver *et al.*, 2011). One of the techniques developed to analyze the relative velocity variations of a medium is the wavelet cross-spectrum technique (Mao *et al.*, 2020). This technique accounts for the travel-time shifts between two traces with high resolution in both frequency and time. The wavelet analysis proposes studying nonstationary signals through decomposition in the time–frequency domain and extracting localized time–frequency characteristics. As a result, the wavelet technique is characterized by higher accuracy, stability, and frequency resolution than other commonly used techniques, for example, the stretching technique (Lobkis and Weaver, 2003) or multiple windows cross-spectrum (Clarke *et al.*, 2011).

We focus our analysis on the seismic sources originating from the volcano dynamics. Through a visual inspection of the records at MLZ station, we select the frequencies for which persistent higher seismic energy is present (see Fig. S3). Then, we set the processing frequency range at 0.8–2.0 Hz to be well above the microseism band.

We apply a processing sequence based on a single-station approach (see details in Figs. S3–S9), in which the correlations between the components of a three-component broadband station are computed. We use phase correlations and phase-weighted stacking (Schimmel and Paulssen, 1997; Schimmel, 1999) to obtain daily cross-component correlations. Because the directionality of the propagating seismic energy can affect the computed relative seismic velocity variations, we analyze the dominant propagation directions for MLZ during the period we look at, obtaining that roughly east–west (EW) and north–south (NS) are the dominant directions (see Fig. S5). We then

TABLE 1
Pearson Correlation Coefficients between the Four Seismic Parameters Analyzed

	1/RSAM	FI	*dv/v*	f_0	Temp	Precip
1/RSAM	1.0	−0.08	0.35	0.03	0.73	−0.20
FI		1.0	0.08	−0.30	−0.02	0.01
dv/v			1.0	0.44	0.23	−0.11
f_0				1.0	−0.22	0.14
Temp					1.0	−0.28
Precip						1.0

For the computation of the values, the filtered time series were used. *dv/v*, relative seismic velocity variations; f_0, fundamental frequency; FI, frequency index; 1/RSAM, reciprocal of the real-time seismic amplitude measurement; the weather variables: Precip, precipitation; and Temp, temperature.

calculate daily relative velocity variations in the time–frequency domain for both dominant directions using the wavelet cross-spectrum technique (Mao *et al.*, 2020).

The resulting relative velocity variations obtained for daily correlations polarized along both the NS and the EW directions are generally coherent with each other (see Fig. S8). We consider the average of the results for the NS and EW directions to represent the actual relative velocity variations around the station. In Figure 2d, a curve indicates a median moving average (using a 7-day window) fit of the results.

Our results are contemporaneous to the eruptive episodes at Copahue in the period 2018–2021, that is, ash and gas emissions as well as incandescence at the crater. The relative velocity-variation curve indicates a systematic alternating behavior between a first period of decreasing values (i.e., a preparation phase) preceding a second period (i.e., an activity phase), starting with the occurrence of ash emissions and during which the velocity values change. However, this pattern along the resulting relative velocity variation (*dv/v*) curve is missing or unclear previous to the ash emissions in November 2022.

Variations of the weather parameters (like precipitations and temperature) are known to affect the overall physical conditions of the subsurface that are manifested as *dv/v* variations (Wang *et al.*, 2017; Feng *et al.*, 2021). Furthermore, the *dv/v* variations describe the subsurface down to 1 km depth (see Fig. S9); thus, the *dv/v* curve is affected by variations in the dynamics of the hydrothermal system, which are influenced by changes in the seasonal weather conditions. However, these conditions do not explain all the variations along the complete *dv/v* curve. Even though the maximum and minimum values along the temperature and precipitations are regular over the years, we observe different shifts of the *dv/v* curve for different temperature and precipitation maximum (minimum) and minimum (maximum) values, respectively. These shifts are correlated to the eruptive phenomena observed at the surface. Specifically, maximum *dv/v* values occur within 2 months after the ash columns in 2018, 2019, and 2020, whereas the maximum temperatures and minimum precipitations occur 2–4 months later; the minimum *dv/v* values occur within 2 months from the ash column of June 2020 and of July 2021, whereas the minimum temperatures and maximum precipitations occur ∼6 months earlier and ∼2 months later, respectively. Therefore, we interpret that important *dv/v* variations are relevant to eruptive processes.

Joint results

Figure 2 shows the results obtained for the evaluated seismic parameters, that is, fundamental frequency, frequency index, 1/RSAM, and relative velocity variations. Note that even though there are six value gaps in *dv/v*, there are only three gaps in f_0, frequency index, and 1/RSAM. The gaps that occurred in September 2018 and August 2019 are shared between the curves and relevant to the absence of seismic data. The following gaps are relevant to alternating availability of data due to instrumental issues (i.e., June 2022) or to nonconvergent *dv/v* results (in February 2020, July 2020, July 2022, and December 2022) or f_0 results (in July 2022). The gaps are longer in *dv/v*, because the resulting curve is computed by fitting the results obtained for the dominant directions of propagation using a 7-day running window.

Our results show that all the seismic parameters correlate to the eruptive phenomena observed at the surface, that is, ash emissions and incandescence. During the analyzed period, changes along both 1/RSAM and *dv/v* curves are gradual, showing the minimum before or during ash emissions and incandescence, and the maximum after the eruptive phenomena. Our results indicate a notable correlation (see Table 1) between 1/RSAM and *dv/v* parameters, the eruptive phenomena observed on the surface and the meteorological parameters. However, the *dv/v* curve is less correlated with the seasonal weather parameters, with local maxima within 2 months after the ash emissions and minima occurring up to 2 months earlier than those ash emissions. These results suggest that, although 1/RSAM is dominated by the physical variations in the hydrothermal system caused by changes in seasonal weather conditions, variations in the *dv/v* values are not (only) affected by these changes, being more sensitive to eruptive phenomena.

On the other hand, f_0 values correlate to intervals of inflation and subsidence (Astort *et al.*, 2024), and both f_0 and frequency index parameters correlate to several eruptive events that occurred in the analyzed period. Patterns along the f_0 and frequency index curves are characterized by an increase in their values; however, the rate of this variation is different for each parameter. f_0 shows a rapid variation months before the volcanic events in September 2019 and November 2022; the frequency index curve gradually increases after the local minimum and before the ash emissions and incandescence in 2019–2022.

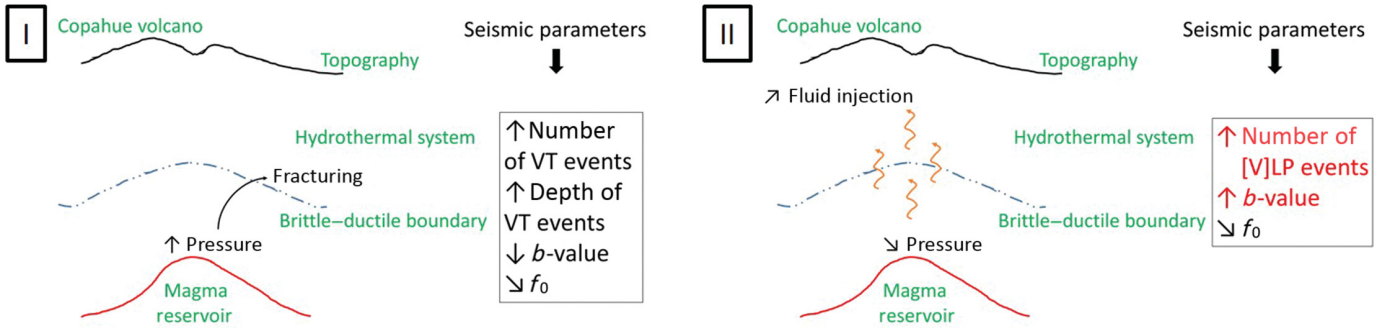

Figure 5. Noncyclical processes of the physical model for Copahue volcano for the period 2018–2023. Temporary ordered stages indicate the evolution of the system. The arrows indicate whether a variable is increasing (↑,↗) or decreasing (↓,↘). A change in a seismic parameter from one stage to another is indicated with red letters. f_0, fundamental frequency; [V]LP, [very-] long-period events; and VT, volcanotectonic events. For the analysis of the noncyclical processes, we use information about the evolution of the number of VT events, their depths, the number of LP events, and the *b*-value; these time series can be found in Farias *et al.* (2023).

The f_0 values show an abrupt increase by May 2019. This feature occurs within a month before a transient drop of the frequency index and during a decrease of both 1/RSAM and the relative velocity variations. Note that the abrupt decrease of the frequency index is indicated with a dashed rectangle in Figure 2 because this is an anomalous feature along the frequency index curve in the period 2018–2023. Given the gap of data that occurred two weeks before the ash emissions started by September 2019, we think that this feature may correspond to the same pattern distinguished for this parameter before other eruptive events in the analyzed period but with a missing maximum. After that, 1/RSAM and the relative velocity variations kept on decreasing until the ash columns were observed by September 2019.

After the increase of 1/RSAM and *dv/v* during the ash emissions from September to November 2019, a new interval of decreasing values starts until the new ash emissions in June 2020. During this time interval, no anomalous variations were observed along the f_0, which kept on decreasing when the frequency index showed a gentle increase in its values. Because the increase is not steep, we use a dashed rectangle to mark this interval in Figure 2. During the ash columns observed in the interval June to September 2020, 1/RSAM keeps decreasing, *dv/v* increases, and no significant changes occur along the f_0 and the frequency index curves.

Within 2 months after the ash emissions culminating in September 2020, the *dv/v* values start to decrease until they reach their local minimum around a month after the ash emission in July 2021. On the other hand, the 1/RSAM values keep on increasing for 4 months, decreasing after that period down to their local minimum by mid-July 2021. Furthermore, the f_0 values decrease during this period, when the frequency index values show a local maximum simultaneous to the start of the incandescence in June 2021.

The interval between October 2021 and November 2022 (the start of the next eruptive phase) is characterized by a gradual decrease of the 1/RSAM values between a new local maximum in January 2022 and a local minimum in August 2022, before the ash emissions in November 2022. This period also exhibits an abrupt variation of the f_0 values by July 2022 and the maximum in the frequency index curve coinciding with the start of the ash columns (note the high similarity between this feature and the one observed before the ash emissions in 2019, 2020, and 2021). Furthermore, the pattern observed in *dv/v* during the previous eruptive events is not present in 2022 and 2023, showing no clear maxima and minima and, therefore, no anomalous variations before the ash emissions in November 2022.

The period between April and December 2023 exhibits anomalously high-transient f_0 values (dashed rectangle in Fig. 2a), showing a median 0.2 Hz higher than the period April 2018–April 2022; the 1/RSAM shows similar variations to previous years, when the frequency index and *dv/v* curves indicate no anomalous values for this period.

Interpretation and Discussion

We combine the results obtained from the analyzed seismic parameters and the subsurface models proposed for the Copahue volcano (Agusto and Vélez, 2017; Carbajal *et al.*, 2022; Farias *et al.*, 2023; Astort *et al.*, 2024) to suggest a physical model that describes the processes leading to the eruptive events in the period 2019–2023. This model consists of a combination of noncyclical and cyclical processes, see Figures 5 and 6, respectively. Cyclical processes are strongly influenced by seasonal weather variations that affect the shallow dynamics of the volcanic system causing the phreatic eruptive events recorded in 2019–2023 (Carbajal *et al.*, 2022). Contrary to that, noncyclical processes are dominated by the dynamics of the deep magmatic system, comprising deep pressure variations, fracturing, deep magma movement, and affecting fluid flows at the depths of the hydrothermal system (Farias *et al.*, 2023).

Noncyclical processes

The location and nature of the seismic events recorded around Copahue volcano (SEGEMAR, 2024; SERNAGEOMIN, 2024),

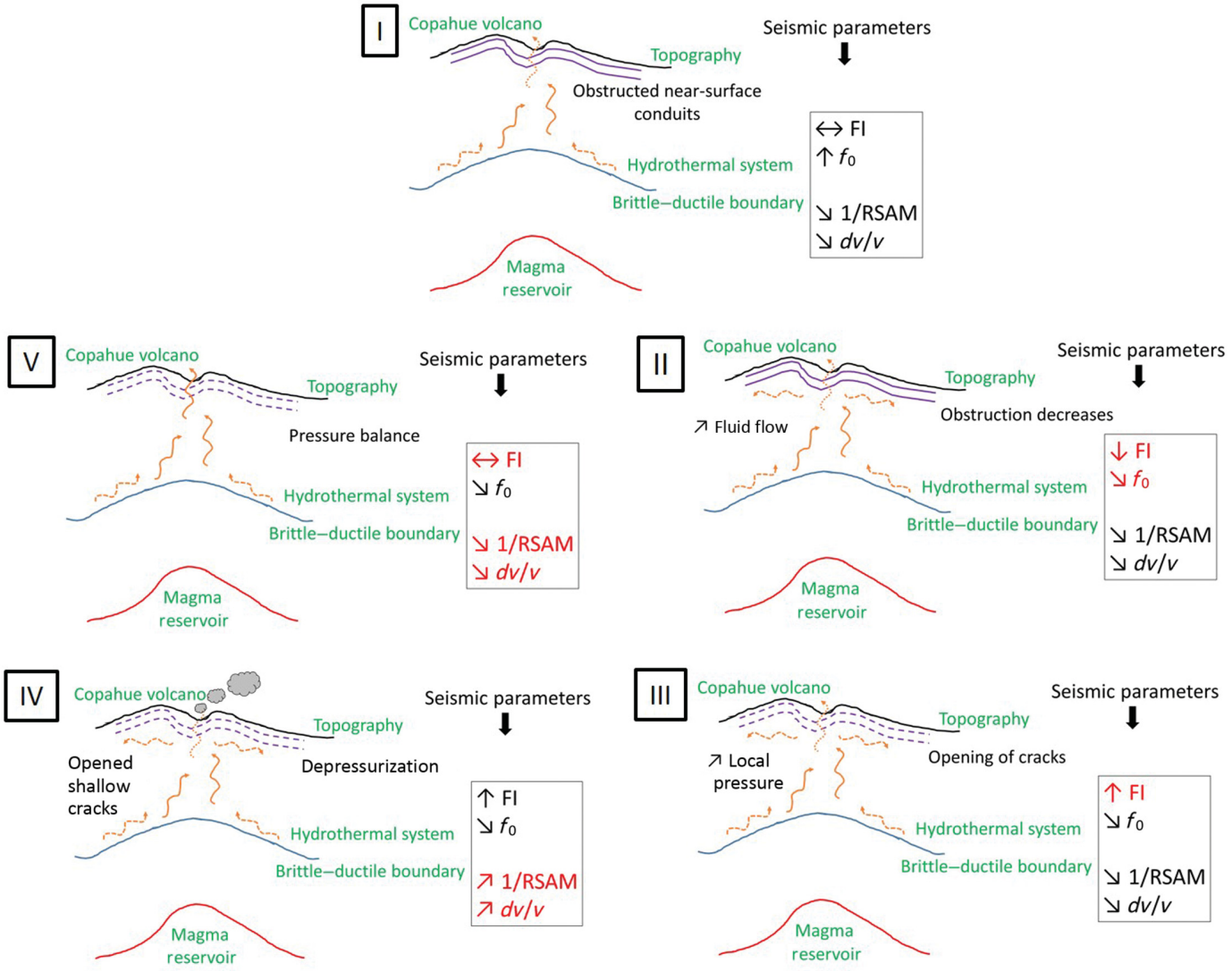

Figure 6. Cyclical processes of the physical model for the eruptive events occurred in the period 2018–2023 at Copahue volcano. Temporary ordered stages indicate the evolution of the system. The arrows indicate whether a variable is increasing (↑,↗), decreasing (↓,↘), or invariant (↔). A change in a seismic parameter from one stage to another is indicated with red letters.*dv/v* indicates relative seismic velocity variations; FI, frequency index; f_0, fundamental frequency; and RSAM, real-time seismic amplitude measurement. The dashed (solid) curves indicate nonobstructed (obstructed) near-surface conduits.

the *b*-value results (Farias *et al.*, 2023), the deformation measurements (Astort *et al.*, 2024), as well as a dissimilar median f_0 value before and after 2021 support the noncyclical dynamics (Fig. 5). The noncyclical processes occur during an interval of inflation (Astort *et al.*, 2024), which is characterized by a lower rate of the f_0 curve and higher-f_0 values. These processes are originated by pressure perturbations at the depths of the magmatic reservoir, which causes sufficiently large variations in the stress state of the volcanic system and triggers the seismic events associated to rock fracturing (VT) (Wassermann, 2012; Farias *et al.*, 2023). Then, seismic events evidence fluid flow at depth (that is, very-long-period [VLP] and/or LP events) (SEGEMAR, 2024; SERNAGEOMIN, 2024), likely through newly-opened pathways toward the surface (even though the surface might not be reached).

Cyclical processes. The seismic parameters we analyze here also provide evidence to support the mechanisms comprising the cyclical processes (Fig. 6). The cyclical circuit starts with the processes leading to an increase of f_0 values (stage I in Fig. 6). This increase evidences a stiffer subsurface. Then, based on a model proposed for the area (Carbajal *et al.*, 2022), we interpret this feature as caused by an obstruction of the near-surface conduits, probably caused by chemical precipitation at shallow depths. This obstruction of the shallow conduits increases the fluid pressure and affects the flow of fluids in the hydrothermal system because of the change in the pressure conditions of the system at these depths (stage II in Fig. 6). An increased pressure gradient

would increase the fluid flow, causing a transient dominance of the seismic energy recorded at lower frequencies relative to that at higher frequencies. Therefore, the frequency index values decrease.

Because of the increase in the subsurface pore pressure, the effective stress in the rock decreases; the elastic moduli of the subsurface are reduced, causing a decrease in *dv/v* values (stage III). This condition promotes a process of opening the cracks at these shallow depths. We interpret that a fast opening of the cracks occurs, so that larger seismic energy at higher frequencies is generated, leading to a transient increase in the frequency index values (Bolton *et al.*, 2022). The roughly monotonous increase along the frequency index curve before the ash emissions may indicate an increase in the magnitude of the openings caused by the higher pressure of the system and/or an increase of the number of cracks being opened.

In stage IV, the sufficiently opened shallow fissures cause depressurization of the system, leading to an eruptive phase. This stage is characterized by increasing 1/RSAM values and increasing *dv/v* values, which is caused by a relaxation of the system during the ash emissions together with an increase in the effective stress due to a reduction in the pore pressure.

The last stage of the circuit is stage V. At this stage the hydrothermal system starts to recover because the ash emissions concluded. Then, both the 1/RSAM and the *dv/v* values decrease. Furthermore, no major fluid flows or crack openings occur in the shallow subsurface, and therefore the frequency index values do not show significant variations.

Note that the proposed physical model describes the eruptive events characterized by variations in the analyzed four seismic parameters. However, the eruptive events that started in June 2020 and July 2021 lack a previous distinguishable variation along the f_0 curve. We relate this to the occurrence of a physical process with sufficiently low energy to be below the detection threshold for this parameter. Both the cyclical and noncyclical processes occur during a decreasing trend of the f_0 values in the period 2019–2023; we interpret this feature as relevant to a gradual decrease of the stress in the system, likely caused by a decreasing volcanic stress field and/or a regional structural relaxation (Walter *et al.*, 2007; Vargas-Bracamontes and Neuberg, 2012). The period April–December 2023 exhibits unique features along f_0, the frequency index, and the *dv/v* parameters, whereas 1/RSAM indicates variations similar to those of the previous years. We recommend continuing to describe the evolution of these parameters to identify the physical causes of the variations over this time period. A next step in this work is to implement the applied methodology to the seismic data recorded at other stations deployed in the area of the Copahue volcano to perform a joint interpretation of the processes occurred at the system.

Conclusions

We analyzed the evolution of magmatic activity at the Copahue volcano—one of the highest-risk volcanoes along the international border between Argentina and Chile between April 2018 and December 2023. Using the complete seismic data recorded by a three-component station deployed near Copahue, we analyzed the resonance frequency, the RSAM, the frequency index, and the relative seismic velocity (*dv/v*) variations. The values of resonance frequency correlate to intervals of inflation and subsidence. Furthermore, rapid increases of the resonance-frequency values split up the period 2018–2023 in four intervals, each one showing decreasing resonance-frequency values; the heights of gas emitted to the surface present minimum values at the boundaries of each interval. In an interval before the eruptive phenomena that occurred at Copahue during the analyzed period, the frequency index curve shows a local minimum followed by a local maximum, which we interpreted as originated by an increase of the flow of fluids followed by a process of opening of cracks. RSAM and *dv/v* values are correlated to weather parameters (temperature and precipitations) as well as to the eruptive phenomena, indicating minimum values before the ash emissions and maximum values after the ash columns culminate.

Combining our results with previous models for the eruptive phenomena at Copahue, we proposed a physical model explaining the processes leading to the eruptive events occurred in the period 2018–2023. The model is composed of cyclical and noncyclical processes, originated by changes in the shallow dynamics due to seasonal weather variations and an increase of the pressure at the depths of the magmatic reservoir, respectively.

The information we obtained could be helpful as an indication of an imminent change in the level of volcanic activity in new volcanic scenarios. Thus, it is fundamental that similar information be available in real time or near real-time in the future. Such knowledge would be fundamental for a better assessment of possible future scenarios at Copahue by the institutions in charge of the volcano monitoring in Argentina and Chile.

Data and Resources

The seismic records utilized in this work were provided by the Observatorio Argentino de Vigilancia Volcánica (OAVV) and the Observatorio Volcanológico de los Andes del Sur (OVDAS). The data are available upon request to the institutions in charge at oavv@segemar.gov.ar and comunicaciones@sernageomin.cl, respectively, or from the Incorporated Research Institutions for Seismology (IRIS), Data services (https://www.fdsn.org/networks/detail/VV/, https://www.fdsn.org/networks/detail/VC/, last accessed December 2023). Maps were created with Generic Mapping Tools (GMT, v.5.2.1). The processing was performed by combining the ObsPy Python-based programming package and GNU Fortran. Horizontal-to-vertical spectral ratio (HVSR) processing was performed using the algorithms provided by *hvsrpy*—a freely-available

Python package. The supplemental material provides figures showing the resulting HVSR calculations for two arbitrarily chosen days; the nonfiltered obtained results; and further details of the processing sequence applied for the computation of the relative seismic velocity variations.

Declaration of Competing Interests

The authors acknowledge that there are no conflicts of interest recorded.

Acknowledgments

The authors thank Fabricio Carbajal and Nicolas Vigide for important discussions and comments that improved the article. The authors thank an anonymous reviewer and Jesús M. Ibañez for their insightful contributions to the present article.

References

Acerra, C., G. Aguacil, A. Anastasiadis, K. Atakan, R. Azzara, P.-Y. Bard, R. Basili, E. Bertrand, B. Bettig, F. Blarel, *et al.* (2004). Guidelines for the implementation of the H/V spectral ratio technique on ambient vibrations measurements, processing and interpretation, *European Commission–EVG1-CT-2000-00026 SESAME*, available at https://sesame.geopsy.org/Papers/HV_User_Guidelines.pdf (last accessed February 2024).

Agusto, M. R., and M. L. Vélez (2017). Avances en el conocimiento del sistema volcánico-hidrotermal del Copahue: A 100 años del trabajo pionero de don pablo groeber, *Rev. Assoc. Geol. Argent.* **74,** no. 1, 109–124 (in Spanish).

Agusto, M., M. Velez, P. Euillades, F. Tassi, A. Caselli, M. Lamberti, J. Szentiványi, J. Llano, V. Nogués, and A. Trinelli (2018). Correlación entre cambios geoqumicos y deformación en el volcán Copahue (Argentina) durante el ciclo eruptivo 2012-2017, *Foro Internacional: Los Volcanes y su impacto*, 31–35, available at https://repositorio.ingemmet.gob.pe/bitstream/20.500.12544/1441/1/2018-Resumenes_Foro_inter_los_volcanes_impacto.pdf (last accessed February 2024) (in Spanish).

Agusto, M. R., A. Caselli, R. Daga, J. Varekamp, A. Trinelli, M. D. S. Afonso, M. L. Velez, P. Euillades, and S. R. Guevara (2017). *The Crater Lake of Copahue Volcano (Argentina): Geochemical and Thermal Changes Between 1995 and 2015*, Vol. 437, Geological Society, London, Special Publications, 107–130.

Aspinall, W., and R. Blong (2015). Chapter 70–Volcanic risk assessment, in *The Encyclopedia of Volcanoes*, Second Ed., H. Sigurdsson (Editor), Academic Press, Amsterdam, The Netherlands, 1215–1231.

Astort, A., F. Carballo, M. Pardo Duró, E. Wright, C. Mardones Castro, A. Alarcón, and G. Acosta (2024). Last unrest of Copahue volcano from geodetic data, *Proc. of the XII Cities on Volcanoes*, Antigua Guatemala, Guatemala, 11–17 February 2024.

Barcelona, H., D. Yagupsky, N. Vigide, and M. Senger (2019). Structural model and slip-dilation tendency analysis at the Copahue geothermal system: Inferences on the reservoir geometry, *J. Volcanol. Geoth. Res.* **375,** 18–31.

Battaglia, J., V. Ferrazzini, T. Staudacher, K. Aki, and J.-L. Cheminée (2005). Pre-eruptive migration of earthquakes at the piton de la Fournaise volcano (Réunion island), *Geophys. J. Int.* **161,** no. 2, 549–558.

Bolton, D. C., S. Shreedharan, G. C. McLaskey, J. Rivière, P. Shokouhi, D. T. Trugman, and C. Marone (2022). The high-frequency signature of slow and fast laboratory earthquakes, *J. Geophys. Res.* **127,** no. 6, e2022JB024170, doi: 10.1029/2022JB024170.

Bour, M., D. Fouissac, P. Dominique, and C. Martin (1998). On the use of microtremor recordings in seismic microzonation, *Soil Dynam. Earthq. Eng.* **17,** no. 7, 465–474.

Bueno, A., R. Balestriero, S. De Angelis, M. C. Benítez, L. Zuccarello, R. Baraniuk, J. M. Ibáñez, and M. V. de Hoop (2021). Recurrent scattering network detects metastable behavior in polyphonic seismo-volcanic signals for volcano eruption forecasting, *IEEE Trans. Geosci. Remote Sens.* **60,** 1–23.

Bueno, A., C. Benítez, S. De Angelis, A. D. Moreno, and J. M. Ibáñez (2019). Volcano-seismic transfer learning and uncertainty quantification with Bayesian neural networks, *IEEE Trans. Geosci. Remote Sens.* **58,** no. 2, 892–902.

Buurman, H., M. E. West, J. Power, and M. Coombs (2006). Seismic precursors to volcanic explosions during the 2006 eruption of Augustine volcano: Chapter 2 in the 2006 eruption of Augustine volcano, Alaska, *U.S. Geol. Surv. Profess. Pap.1769-2*, doi: 10.3133/pp17692.

Cabrera-Pérez, I., L. D'Auria, J. Soubestre, M. Przeor, J. Barrancos, R. García-Hernández, J. M. Ibáñez, I. Koulakov, D. M. van Dorth, V. Ortega, *et al.* (2023). Spatio-temporal velocity variations observed during the pre-eruptive episode of La Palma 2021 eruption inferred from ambient noise interferometry, *Sci. Rep.* **13,** no. 1, 12039, doi: 10.1038/s41598-023-39237-9.

Carbajal, F., N. Vigide, G. Badi, M. Agusto, S. Garcia, and M. Lamberti (2022). Variation of the copahue volcano crater lake and its relation with gas and ash emissions during 2019-2021, *Proc. of the XIV Commission-on-the-Chemistry-of-Volcanic-Gases Gas Workshop*, Arequipa, Peru, 6–16 November 2022.

Caselli, A., M. Agusto, M. Velez, P. Forte, C. Bengoa, R. Daga, J. Albite, and B. Capaccioni (2016). *The 2012 Eruption*, Springer, Berlin, Heidelberg, 61–77, doi: 10.1007/978-3-662-48005-2_4.

Caselli, A. T., C. Liccioli, and F. Tassi (2016). *Risk Assessment and Mitigation at Copahue Volcano*, Springer, Berlin, Heidelberg, 239–254, doi: 10.1007/978-3-662-48005-2_10.

Chardot, L., A. D. Jolly, B. M. Kennedy, N. Fournier, and S. Sherburn (2015). Using volcanic tremor for eruption forecasting at white island volcano (Whakaari), New Zealand, *J. Volcanol. Geoth. Res.* **302,** 11–23.

Cipta, A., P. Cummins, J. Dettmer, E. Saygin, M. Irsyam, A. Rudyanto, and J. Murjaya (2018). Seismic velocity structure of the Jakarta basin, Indonesia, using trans-dimensional Bayesian inversion of horizontal-to-vertical spectral ratios, *Geophys. J. Int.* **215,** no. 1, 431–449.

Clarke, D., L. Zaccarelli, N. Shapiro, and F. Brenguier (2011). Assessment of resolution and accuracy of the moving window cross spectral technique for monitoring crustal temporal variations using ambient seismic noise, *Geophys. J. Int.* **186,** no. 2, 867–882.

Climate-Hazards-Center (2020). CHIRTSdaily, Climate Hazards Center, doi: 10.15780/G2008H.

Cornelius, R. R., and B. Voight (1994). Seismological aspects of the 1989–1990 eruption at redoubt volcano, alaska: The materials failure forecast method (FFM) with RSAM and SSAM seismic data, *J. Volcanol. Geotherm. Res.* **62,** nos. 1/4, 469–498.

Cornelius, R. R., and B. Voight (1996). Real-time seismic amplitude measurement (RSAM) and seismic spectral amplitude measurement (SSAM) analyses with the materials failure forecast method (FFM), June 1991 explosive eruption at Mount Pinatubo, in *Fire and Mud: Eruptions and Lahars of Mount Pinatubo*, C. G. Newhall and R. S. Punongbayan (Editors), University of Washington Press, Seattle, Washington, and Philippines, 249–268.

Cortés, G., M. C. Benitez, L. García, I. Álvarez, and J. M. Ibanez (2015). A comparative study of dimensionality reduction algorithms applied to volcano-seismic signals, *IEEE J. Sel. Top. Appl. Earth Obs. Remote Sens.* **9,** no. 1, 253–263.

Cox, B. R., T. Cheng, J. P. Vantassel, and L. Manuel (2020). A statistical representation and frequency-domain window-rejection algorithm for single-station HVSR measurements, *Geophys. J. Int.* **221,** no. 3, 2170–2183.

Elissondo, M., and C. Farıas (2024). Riesgo Volcánico Relativo en Territorio Argentino, Buenos Aires, Servicio Geológico Minero Argentino. Instituto de Geología y Recursos Minerales, available at https://repositorio.segemar.gov.ar/handle/308849217/4417 (last accessed May 2024).

Endo, E. T., and T. Murray (1991). Real-time seismic amplitude measurement (rsam): A volcano monitoring and prediction tool, *Bull. Volcanol.* **53,** no. 7, 533–545.

Ewert, J. W., and D. A. Swanson (1992). Monitoring volcanoes: Techniques and strategies used by the staff of the Cascades Volcano Observatory, 1980-90, *U.S. Geol. Surv. Numbered Series 1966*, U.S. Government Printing Office.

Farias, C., J. Lazo, D. Basualto, M. Saavedra, F. Muñoz-Quiroz, L. Zuñiga-Urrea, R. Martínez-Bravo, I. Huentenao-Inostroza, and R. Saéz-Opazo (2023). One decade of *b*-value variations from volcano-tectonic seismicity as an early indicator of episodes of crisis in a volcano: The case of Copahue, southern Andes, *Front. Earth Sci.* **11,** 1181177, doi: 10.3389/feart.2023.1181177.

Feng, K.-F., H.-H. Huang, Y.-J. Hsu, and Y.-M. Wu (2021). Controls on seasonal variations of crustal seismic velocity in Taiwan using single-station cross-component analysis of ambient noise interferometry, *J. Geophys. Res.* **126,** no. 11, e2021JB022650, doi: 10.1029/2021JB022650.

Folguera, A., E. R. Vera, L. Vélez, J. Tobal, D. Orts, M. Agusto, A. Caselli, and V. Ramos (2016). A review of the geology, structural controls, and tectonic setting of Copahue volcano, southern volcanic zone, Andes, Argentina, in *Copahue Volcano*, F. Tassi, O. Vaselli, and A. Tomas Caselli (Editors), Vol. 2016, Springer, Heidelberg, 3–22.

Funk, C., P. Peterson, M. Landsfeld, D. Pedreros, J. Verdin, S. Shukla, G. Husak, J. Rowland, L. Harrison, A. Hoell, *et al.* (2015). The climate hazards infrared precipitation with stations—A new environmental record for monitoring extremes, *Sci. Data* **2,** no. 1, 1–21.

Girona, T., C. Caudron, and C. Huber (2019). Origin of shallow volcanic tremor: The dynamics of gas pockets trapped beneath thin permeable media, *J. Geophys. Res.* **124,** no. 5, 4831–4861.

Gosar, A. (2017). Study on the applicability of the microtremor HVSR method to support seismic microzonation in the town of Idrija (W Slovenia), *Nat. Hazards Earth Syst. Sci.* **17,** no. 6, 925–937, doi: 10.5194/nhess-17-925-2017.

Gutenberg, B., and C. F. Richter (1944). Frequency of earthquakes in California, *Bull. Seismol. Soc. Am.* **34,** no. 4, 185–188.

Ibáñez, J., E. Del Pezzo, C. Bengoa, A. Caselli, G. Badi, and J. Almendros (2008). Volcanic tremor and local earthquakes at Copahue volcanic complex, southern Andes, Argentina, *J. Volcanol. Geoth. Res.* **174,** no. 4, 284–294.

Ketner, D., and J. Power (2013). Characterization of seismic events during the 2009 eruption of redoubt volcano, Alaska, *J. Volcanol. Geotherm. Res.* **259,** 45–62.

Khalili, M., and A. V. Mirzakurdeh (2019). Fault detection using microtremor data (HVSR-based approach) and electrical resistivity survey, *J. Rock Mech. Geotech. Eng.* **11,** no. 2, 400–408.

Kumagai, H., M. Nakano, T. Maeda, H. Yepes, P. Palacios, M. Ruiz, S. Arrais, M. Vaca, I. Molina, and T. Yamashima (2010). Broadband seismic monitoring of active volcanoes using deterministic and stochastic approaches, *J. Geophys. Res.* **115,** no. B8, doi: 10.1029/2009JB006889.

Le Breton, M., N. Bontemps, A. Guillemot, L. Baillet, and Éric Larose (2021). Landslide monitoring using seismic ambient noise correlation: Challenges and applications, *Earth Sci. Rev.* **216,** 103518, doi: 10.1016/j.earscirev.2021.103518.

Lesage, P. (2022). Seismic monitoring of volcanoes and eruption forecasting, in *Hazards and Monitoring of Volcanic Activity 2: Seismology, Deformation and Remote Sensing*, Y. Lagabrielle (Editor), ISTE Ltd–Wiley, London, United Kingdom, 1–93, doi: 10.1002/9781394169610.ch1.

Lobkis, O. I., and R. L. Weaver (2003). Coda-wave interferometry in finite solids: Recovery of p-to-s conversion rates in an elastodynamic billiard, *Phys. Rev. Lett.* **90,** no. 25, 254302, doi: 10.1103/PhysRevLett.90.254302.

Lundgren, P., M. Nikkhoo, S. V. Samsonov, P. Milillo, F. Gil-Cruz, and J. Lazo (2017). Source model for the Copahue volcano magma plumbing system constrained by insar surface deformation observations, *J. Geophys. Res.* **122,** no. 7, 5729–5747.

Machacca, R., P. Lesage, H. Tavera, J. D. Pesicek, C. Caudron, J. L. Torres, N. Puma, K. Vargas, I. Lazarte, M. Rivera, *et al.* (2023). The 2013–2020 seismic activity at sabancaya volcano (peru): Long lasting unrest and eruption, *J. Volcanol. Geoth. Res.* **435,** 107767, doi: 10.1016/j.jvolgeores.2023.107767.

Mao, S., A. Mordret, M. Campillo, H. Fang, and R. D. van der Hilst (2020). On the measurement of seismic traveltime changes in the time–frequency domain with wavelet cross-spectrum analysis, *Geophys. J. Int.* **221,** no. 1, 550–568.

McNutt, S. R. (2005). Volcanic seismology, *Annu. Rev. Earth Planet. Sci.* **32,** 461–491.

Moore, J. R., P. R. Geimer, R. Finnegan, and M. S. Thorne (2018). Use of seismic resonance measurements to determine the elastic modulus of freestanding rock masses, *Rock Mech. Rock Eng.* **51,** 3937–3944.

Mundepi, A., C. Lindholm, and Kamal (2009). Soft soil mapping using horizontal to vertical spectral ratio (HVSR) for seismic hazard assessment of Chandigarh city in Himalayan foothills, North India, *J. Geol. Soc. India* **74,** 551–558.

Nakamura, Y. (1989). A method for dynamic characteristics estimation of subsurface using microtremor on the ground surface, *Q Rep. Railway Tech. Res. Inst.* **30,** 25–33.

Nishitsuji, Y., E. Ruigrok, M. Gomez, and D. Draganov (2014). Global-phase H/V spectral ratio for delineating the basin in the Malargüe region, Argentina, *Seismol. Res. Lett.* **85,** no. 5, 1004–1011.

Obermann, A., T. Planès, E. Larose, and M. Campillo (2013). Imaging pre-eruptive and coeruptive structural and mechanical changes of a volcano with ambient seismic noise, *J. Geophys. Res.* **118,** no. 12, 6285–6294.

Okamoto, K., and S. Tsuno (2018). Numerical studies of effects of dipping structures on horizontal/vertical spectral ratios, *Pure Appl. Geophys.* **175,** 2837–2852.

Okamoto, K., H. Asanuma, and H. Nimiya (2021). Fluid activity detection in geothermal areas using a single seismic station by monitoring horizontal-to-vertical spectral ratios, *Sci. Rep.* **11,** no. 1, 8372, doi: 10.1038/s41598-021-86775-1.

Pallister, J., and S. R. McNutt (2015). Synthesis of volcano monitoring, in *The Encyclopedia of Volcanoes*, H. Sigurdsson (Editor), Academic Press, Amsterdam, 1151–1171, doi: 10.1016/B978-0-12-385938-9.00066-3.

Papale, P. (2020). *Forecasting and Planning for Volcanic Hazards, Risks, and Disasters*, Elsevier, Amsterdam, The Netherlands.

Qamar, A. I., S. D. Malone, S. C. Moran, W. P. Steele, W. A. Thelen, D. Sherrod, W. Scott, and P. Stauffer (2008). Near-real-time information products for Mount St. Helens—Tracking the ongoing eruption. A volcano Rekindled: The renewed eruption of Mount St. Helens, 2004–2006, 61–70, doi: 10.3133/pp17503.

Rey-Devesa, P., C. Benítez, J. Prudencio, L. Gutiérrez, G. Cortés-Moreno, M. Titos, I. Koulakov, L. Zuccarello, and J. M. Ibáñez (2023). Volcanic early warning using Shannon entropy: Multiple cases of study, *J. Geophys. Res.* **128,** no. 6, e2023JB026684, doi: 10.1029/2023JB026684.

Rey-Devesa, P., J. Prudencio, C. Benítez, M. Bretón, I. Plasencia, Z. León, F. Ortigosa, L. Gutiérrez, R. Arámbula-Mendoza, and J. M. Ibáñez (2023). Tracking volcanic explosions using Shannon entropy at Volcán de Colima, *Sci. Rep.* **13,** no. 1, 9807, doi: 10.1038/s41598-023-36964-x.

Rivera, J. A., G. Marianetti, and S. Hinrichs (2018). Validation of chirps precipitation dataset along the central Andes of Argentina, *Atmos. Res.* **213,** 437–449.

Satoh, T., H. Kawase, T. Iwata, S. Higashi, T. Sato, K. Irikura, and H.-C. Huang (2001). S-wave velocity structure of the Taichung Basin, Taiwan, estimated from array and single-station records of microtremors, *Bull. Seismol. Soc. Am.* **91,** no. 5, 1267–1282.

Scarpa, R., R. I. Tilling, and B. Chouet (1996). New methods and future trends in seismological volcano monitoring, in *Monitoring and Mitigation of Volcano Hazards*, Springer, Berlin, Germany, 23–97, ISBN: 978-3-64280087.

Schimmel, M. (1999). Phase cross-correlations: Design, comparisons, and applications, *Bull. Seismol. Soc. Am.* **89,** no. 5, 1366–1378.

Schimmel, M., and H. Paulssen (1997). Noise reduction and detection of weak, coherent signals through phase-weighted stacks, *Geophys. J. Int.* **130,** no. 2, 497–505.

Scholz, C. H. (2015). On the stress dependence of the earthquake *b* value, *Geophys. Res. Lett.* **42,** no. 5, 1399–1402.

SEGEMAR (2024). Observatorio Argentino de Vigilacia Volcánica - Servicio Geológico y Minero Argentino, available at https://oavv.segemar.gob.ar/monitoreo-volcanico/ (last accessed February 2024) (in Spanish).

Sens-Schonfelder, C., and F. Brenguier (2019). Noise-based monitoring, in *Seismic Ambient Noise*, N. Nakata, L. Gualtieri, and A. Fichtner (Editors), Cambridge University Press, Cambridge, United Kingdom, 267–301, doi: 10.1017/9781108264808.011.

SERNAGEOMIN (2024). Red Nacional de Vigilancia Volcánica, Servicio Nacional de Geología y Minería, Chile, available at https://rnvv.sernageomin.cl/ (last accessed February 2024) (in Spanish).

Snieder, R. (2006). The theory of coda wave interferometry, *Pure Appl. Geophys.* **163,** nos. 2/3, 455–473.

Snieder, R., A. Grêt, H. Douma, and J. Scales (2002). Coda wave interferometry for estimating nonlinear behavior in seismic velocity, *Science* **295,** no. 5563, 2253–2255.

Sparks, R., J. Biggs, and J. Neuberg (2012). Monitoring volcanoes, *Science* **335,** no. 6074, 1310–1311.

Sparks, R. S. J. (2003). Forecasting volcanic eruptions, *Earth Planet. Sci. Lett.* **210,** nos. 1/2, 1–15.

Stern, R. J. (2002). Subduction zones, *Rev. Geophys.* **40,** no. 4, 3-1–3-38.

Tardani, D., E. Roulleau, D. L. Pinti, P. Pérez-Flores, L. Daniele, M. Reich, P. Sanchez-Alfaro, D. Morata, and L. Richard (2021). Structural control on shallow hydrogeochemical processes at Caviahue-Copahue volcanic complex (CCVC), Argentina, *J. Volcanol. Geoth. Res.* **414,** 107228, doi: 10.1016/j.jvolgeores.2021.107228.

Thompson, G., M. Beer, I. Kougioumtzoglou, E. Patelli, and S. Au (2015). Seismic monitoring of volcanoes, in *Encyclopedia of Earthquake Engineering*, M. Beer, I. A. Kougioumtzoglou, E. Patelli, and I. S.-K. Au (Editors), Springer, Berlin, Heidelberg, Vol. 10, 1–25.

Torrese, P., A. P. Rossi, V. Unnithan, R. Pozzobon, D. Borrmann, H. Lauterbach, E. Luzzi, and F. Sauro (2020). HVSR passive seismic stratigraphy for the investigation of planetary volcanic analogues, *Icarus* **351,** 113970, doi: 10.1016/j.icarus.2020.113970.

Vargas-Bracamontes, D., and J. Neuberg (2012). Interaction between regional and magma-induced stresses and their impact on volcano-tectonic seismicity, *J. Volcanol. Geoth. Res.* **243–244,** 91–96, doi: 10.1016/j.jvolgeores.2012.06.025.

Verdin, A., C. Funk, P. Peterson, M. Landsfeld, C. Tuholske, and K. Grace (2020). Development and validation of the chirts-daily quasi-global high-resolution daily temperature data set, *Sci. Data* **7,** no. 1, 303, doi: 10.1038/s41597-020-00643-7.

Walter, T. R., R. Wang, M. Zimmer, H. Grosser, B. Lühr, and A. Ratdomopurbo (2007). Volcanic activity influenced by tectonic earthquakes: Static and dynamic stress triggering at Mt. Merapi, *Geophys. Res. Lett.* **34,** no. 5, doi: 10.1029/2006GL028710.

Wang, Q.-Y., F. Brenguier, M. Campillo, A. Lecointre, T. Takeda, and Y. Aoki (2017). Seasonal crustal seismic velocity changes throughout Japan, *J. Geophys. Res.* **122,** no. 10, 7987–8002.

Wassermann, J. (2012). Volcano seismology, in *New Manual of Seismological Observatory Practice 2 (NMSOP-2)*, P. Bormann (Editor), Deutsches GeoForschungsZentrum GFZ, Potsdam, Germany, 1–77.

Weaver, R., C. Hadziioannou, E. Larose, and M. Campillo (2011). On the precision of noise correlation interferometry, *Geophys. J. Int.* **185,** 1384–1392.

Xu, R., and L. Wang (2021). The horizontal-to-vertical spectral ratio and its applications, *EURASIP J. Adv. Signal Process.* **2021,** 75, doi: 10.1186/s13634-021-00765-z.

Manuscript received 26 February 2024
Published online 14 June 2024